Available online at www.sciencedirect.com
SCIENCE DIRECT®
Control Engineering Practice 13 (2005) 41–53
CONTROL ENGINEERING PRACTICE
www.elsevier.com/locate/conengprac

Optimal power management of an experimental fuel cell/supercapacitor-powered hybrid vehicle

P. Rodatz*, G. Paganelli, A. Sciarretta, L. Guzzella

Department of Measurement and Control Laboratory, Swiss Federal Institute of Technology Zurich, ETH, Zentrum, ML K36.2, Sonneggstrasse 3, CH-8092 Zürich, Switzerland

Received 12 July 2002; accepted 20 December 2003

Abstract

This paper deals with power flow management within a hybrid fuel cell-powered vehicle during real-time operation. The aim is the real-time control of the power distribution between the fuel cell and its associated energy storage to optimize the global hydrogen consumption while maintaining drivability. An original concept to convert the electrical power flow into equivalent hydrogen cost is proposed. On that basis, the previously developed control strategy (the equivalent consumption minimization strategy) is used to determine the real-time optimal power distribution by simple minimization of a univariate form. The approach presented has been applied to and implemented on a real fuel cell-supercapacitor-powered vehicle. Experimental and simulation results are presented, demonstrating that this approach provides an improvement of fuel efficiency along with robustness and ease of implementation.

Keywords: Electric vehicles; Hybrid vehicles; Energy management systems; Fuel cells; Supervisory control

1. Introduction

Stimulated by the urgent need for more fuel-efficient vehicles that produce fewer harmful emissions, fuel cell-powered vehicles are being investigated in many research and development programs. The combination of a reversible energy storage source with a fuel cell, referred to as *hybridization,* may greatly benefit fuel cell technology. The potential advantages are numerous:

- As the additional energy source can fulfill the transient power demand fluctuations, the fuel cell can be downsized to fit the average power demand.
- The ability of the reversible energy source to recover kinetic energy during regenerative braking leads significant energy savings.
- The hybridization creates additional degrees of freedom in the power flows and thus offers opportunities for the optimization of the vehicle efficiency.

The coordination among the various power sources requires a high level of control in the vehicle, typically referred to as supervisory control. This paper focuses on the management of these power flows at any instance in a vehicle equipped with both fuel cells and supercapacitors.

The technical literature contains several algorithms for the global optimization of energy management systems. They either use the techniques of dynamic programming (Brahma, Guezennec, & Rizzoni, 2000; Lin et al., 2001) or of optimal control (Delprat, Guerra, Paganelli, Lauber, & Delhom, 2001a). All of their results are based on a priori knowledge of the future driving conditions, as provided by scheduled driving cycles. Therefore, they are not suitable for real-time control, but they still have an acknowledged importance as a basis of comparison for the evaluation of the quality of real-time control strategies.

Also the development of a real-time power management control strategy, based on an optimization in real time, has been the subject of investigation (Delprat, Guerra, & Rimaux, 2001b; Seiler & Schröder, 1998; Johnson, Wipke, & Rausen, 2000; Ogburn et al., 2000; Wipke, Markel, & Nelson, 2001). In this approach, often referred as "local optimization", two main constraints must be accounted for: (a) no or very limited a priori knowledge of the future driving conditions is

*Corresponding author. Tel.: +41-163-259-26; fax: +41-163-211-39.
E-mail address: rodatz@imrt.mavt.ethz.ch (P. Rodatz).

0967-0661/$ - see front matter © 2004 Elsevier Ltd. All rights reserved.
doi:10.1016/j.conengprac.2003.12.016

Nomenclature

E^h_{DC}	energy required at the DC link (J)
E_e	time integral of reversible power (J)
E^{eq}_e	fuel energy equivalent of E^f_e (J)
E^f_e	total reversible energy use over driving cycle (J)
E^h_{FC}	electrical energy available from the fuel cell if it were to run at full power over the time horizon t^h (J)
E^0_{H2}	fuel energy required to drive cycle if no reversible path were present (J)
E^f_{H2}	total fuel energy use over driving cycle (J)
E_r	recoverable kinetic energy of vehicle (J)
E_{SC}	energy stored in supercapacitors (J)
J	cost function (dimensionless)
$\dot{m}_{H2}$	hydrogen mass flow rate (kg/s)
p	probability factor (dimensionless)
P_{DC}	power flow in DC link (W)
P^{avg}_{DC}	typical average power demand (W)
P_e	reversible energy use (W)
P_{FC}	net power produced by fuel cell (W)
P^{max}_{FC}	maximum fuel cell power output (W)
P_{H2}	hydrogen power needed for power output P_{FC} (W)
P_{SC}	power to or from supercapacitors (W)
s	equivalence factor (dimensionless)
s_{chg}	equivalence factor when reversible energy storage is charged (dimensionless)
s_{dis}	equivalence factor when reversible energy storage is discharged (dimensionless)
t^h	time horizon (s)
t_k	time step (s)
u	power split factor (dimensionless)

available during the actual operation, and (b) the charge of the reversible energy source must be sustained without external sources, but based only upon fuel conversion or regenerative braking during the vehicle operation. The core of each "local optimization" strategy is the definition of a cost function that is to be minimized, which depends only upon the system variables at that instant time. The cost function has to be a function of the fuel energy use, since its minimization is the main aim of the power management control system, but in the interest of the required charge sustainability, the variations in stored reversible energy have to be taken into account as well.

The various approaches proposed in the literature deal with these aspects in different ways. In some cases, a tuning parameter affecting the optimization is introduced. This parameter is adjusted according to the current state-of-charge (SOC) deviation by means of a PID controller (Delprat et al., 2001b). In other cases, the cost function is the sum of all the losses in the reversible and thermal paths (Seiler & Schröder, 1998). More consistently, the approach presented in Paganelli et al. (2000) and Paganelli, Ercole, Brahma, Guezennec, and Rizzoni (2001) clearly recognized that since the reversible energy and the fuel energy are not directly comparable, an equivalence factor is needed. In that approach, the cost function was evaluated as the sum of the fuel consumption and an equivalent fuel consumption due to the SOC variation (ECMS, Equivalent Consumption Minimization Strategy).

Section 2 describes the experimental vehicle, which has been used to demonstrate the proposed approach. The model used to simulate the power flows and the performance data of this experimental vehicle is presented in Section 3. In Section 4 of this paper, a new method is proposed which evaluates the equivalence factor between fuel and electrical energy for a hybrid powertrain. It does not require any assumptions on the average efficiencies of the various paths, and it is based on a coherent definition of self-sustainability that implies a substantial constancy of the equivalence factors evaluated. Such a definition can be used both for taking into consideration SOC deviations in the evaluation of fuel consumption and for real-time control. Accordingly, its application to the mentioned ECMS power management control strategy is also presented. Section 4 further deals with the implementation of the proposed approach to the considered experimental vehicle. Finally, simulated and experimental results are reported in Section 5.

2. Hy.Power experimental vehicle

The approach presented in this paper was tested on the road using the experimental fuel cell vehicle of the so-called Hy.Power project, which is an ongoing collaboration between the Paul Scherrer Institute (PSI), the Swiss Federal Institute of Technology Zurich (ETHZ) and several industrial partners (Rodatz et al., 2003).

The project was initiated in 1999 with the aim to design and realize a fuel cell-powered electric vehicle with supercapacitors storage. First, a 1 kW test bench was built to investigate basic principles of the fuel cell system. In 2001, a pilot system was realized which included a 6 kW fuel cell system and a 10 kW supercapacitors module (Dietrich et al., 2001). This pilot system was used to test the functionality of the vehicle powertrain. Based upon the knowledge gained from the pilot system, the test vehicle was built in 2002. The vehicle, a Volkswagen Bora (a five-seat sedan

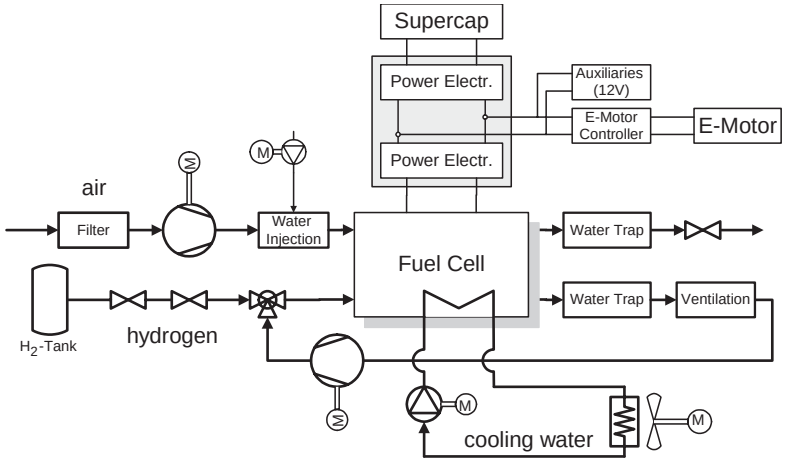

Fig. 1. Outline of fuel cell system.

vehicle known in the US as VW Jetta) was modified to accommodate the new powertrain. It was equipped with two 26 l hydrogen tanks (pressure up to 350 bar) and weighs 1922 kg. The weight is distributed between the vehicle base weight (957 kg), components of the electric motor (incl. inverter, transmission—301 kg), fuel cell system (496 kg) and the supercapacitors (196 kg).

Fuel cells are electrochemical devices, which convert chemical energy into electrical energy directly by oxidizing hydrogen without intermediate thermal or mechanical processes. Proton exchange membrane fuel cells (PEM-FC) also known as polymer electrolyte fuel cells (PEFC) are preferred in automotive applications because they are efficient, compact and of low weight. Since PEFC operate at almost ambient temperatures, the warm-up process is kept short and their ability to follow the dynamic changes in the applied load is given.

The power output of a single cell with an active area of 200 cm^2 is less than 100 W. Numerous cells connected in series form a multi-kW stack, and a system containing several stacks generates a power output of several tens of kW. Altogether, an array of six stacks with 125 cells each was built by PSI and ETHZ, creating a 40-kW fuel cell system.[1] The stacks are electrically connected as two parallel strings of three stacks in series. The reactant gases and the cooling liquid are fed in parallel through a manifold. In addition to the stacks, the auxiliary subsystems of air supply, fuel supply, and coolant were developed by PSI, ETHZ, and FEV Motorentechnik AG. The entire fuel cell system is represented in Fig. 1; Table 1 lists its main parameters.

Supercapacitors are electrical storage devices with a high power and a high energy density. Their energy density is up to 100 times higher than that of conventional capacitors, and their power density is up to 10 times higher than that of batteries. With their wide operating temperature range and their long lifetime, supercapacitors are the short-term storage elements of choice. Jointly developed by PSI and Montena SA, the supercapacitors installed in the vehicle have a rated capacitance of 1600 F with a rated voltage of 2.5 V. Altogether, the 282 pair wise connected supercapacitors yield a storage capacity of 360 Wh and are able to furnish 50 kW for a duration of roughly 15 s (Kötz, Bärtschi, Büchi, Gallay, & Dietrich, 2002). The maximum voltage of the supercapacitors module is 360 V. To equilibrate the cell voltage inside the module and to avoid the overcharging of specific cells an active voltage-balancing unit is mounted on the supercapacitors.

The vehicle is a hybrid vehicle in which the fuel cell acts as the primary power source. The supercapacitors are sized for peak power leveling to assist the fuel cell during hard acceleration. Moreover, the supercapacitors are used to store energy from regenerative braking and they offer an opportunity to optimize the vehicle efficiency. The vehicle is powered by an AC motor with a permanent power output of 45 kW, a peak power output of 75 kW and a maximum torque of 255 N m. The three devices are connected by a DC link (Fig. 2), which is kept at a constant high voltage, thereby

Table 1
Fuel cell system parameters

Parameter	
Number of cells	750 (375 in series)
Active area per cell	204 cm^2
Nominal operating temperature	70°C
Cathode pressure	2 bar_{abs}
Anode pressure	2.2 bar_{abs}
Air utilization[a]	<0.5
Fuel utilization[a]	>0.5

[a] These poor utilization rates result from the need to increase the flow in the channels to assist the liquid water removal and to avoid reactants undersupply during transients.

[1] For simplicity, in the remaining of the paper *fuel cell* will actually refer to as the entire array of six stacks together.

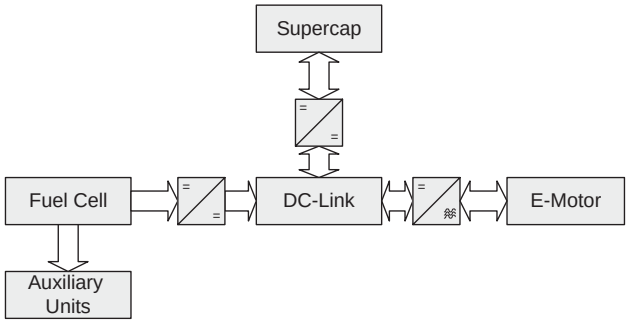

Fig. 2. Powertrain components and power flow.

assuring the highest possible motor torque over the whole speed range. Since the voltage of the fuel cell and supercapacitors are not constant (the former drops with increasing load and the latter with decreasing SOC) DC/DC converters have to be installed in the connection.

Fuel cells and supercapacitors are both passive elements. Their operating point is not directly controllable, thus a current needs to be imposed by a load to draw power from them. This can be either done by directly connecting a variable load or, as in the case of the powertrain considered, by inserting a controlling device such as an electronic power converter in the electric circuit. When a current (flow variable) is imposed, a specific voltage (effort variable) is returned, similarly to a battery. Accordingly, a given fuel cell current results in a hydrogen mass flow by the amount of hydrogen consumed by the fuel cell reaction. Fig. 3 shows the corresponding causality flow chart of the entire powertrain.

The fuel cell voltage is highest when no current is flowing and drops with increasing current due to activation overvoltage and ohmic resistance losses in the membrane. At high currents, the voltage drops sharply as the transport of reactant gases is not able to keep pace with the amount used in the reaction. Consequently, reactant starvation occurs at the reaction side and the cell fails. Since a current is drawn through the stack, the failed cell may start to operate as an electrolytical cell and cause irreversible damage. Therefore, the current that is allowed to be imposed on the fuel cell needs to be limited. The current was limited at 150 A, although the DC/DC converter would have allowed values as high as 250 A.

A lag between the onset of the load on the fuel cell and the response of the reactant supply system results in an undersupply of reactants to the fuel cell, which leads to a breakdown of the chemical reaction and a rapid loss in voltage. This phenomenon may be avoided by restricting the dynamics of the load. In this set-up, the dynamic of the fuel cell system was limited to a conservative 2.5 kW/s. As a further protection, the power demand on the fuel cell is reduced if any stack voltage drops below 70 V and the system is shut down if any stack voltage falls below 60 V.

Last but not the least, the DC/DC converter and the fuel cell were designed for a net power of 40 kW. Unfortunately, the parallel supply of the reactant gases to the six stacks caused more problems than expected. Above 30 kW, the fuel cell voltage was highly unstable. An even fluid distribution to all the flow channels is difficult to achieve, since slight deviations in the flow resistance lead to variations of the flow. At high utilization[2] rates these flow discrepancies translate into variations of the cell voltage across the stack. These discrepancies are assumed to result from liquid water droplets forming in the flow channels and thereby interfering with the gas flow. Therefore, the power was limited to 27 kW to have a proper margin of safety.

The supercapacitors were limited in power and current due to the design of the DC/DC converter to 60 kW and 250 A, respectively. To avoid overcharging the voltage was limited to 360 V for the module or to 2.5 V for each cell. When the supercapacitors are discharged, the voltage decreases and the current has to be increased to achieve a constant power output. The losses due to the internal resistance of the cells increases with square of the current. Hence, at low voltage the efficiency of the supercapacitors is poor ($\eta_{SC} < 50\%$), and the system was operated to remain above 180 V.

When all these constraints due to limitations in voltage, current and power are combined, the momentary maximum power output of the fuel cell and the supercapacitors can be calculated for every time step. The upper boundary value is transmitted to the controller of the electric motor, which restricts the power the motor can draw. Similarly, a lower boundary is used to restrict the regenerative braking when needed. Due to the constraints in the transient behavior of the fuel cell system, the fuel cell power is brought down with a gradient of 5 kW/s. (Only during emergency shutdown the power is brought down immediately.) The energy accumulating during this time must be stored in the supercapacitors. This restriction has to be taken into account when defining the lower boundary. All constraints on the powertrain are summarized in Table 2.

3. Vehicle modeling

The performance of the experimental fuel cell vehicle was evaluated using VP-SIM, a vehicle simulator developed at the Ohio State University over the last few years. VP-SIM is a modular and scalable vehicle simulator programmed in Matlab/Simulink. It is based on an original unified representation of energy and

[2]The hydrogen utilization is defined as the ratio of hydrogen consumed to hydrogen fed.

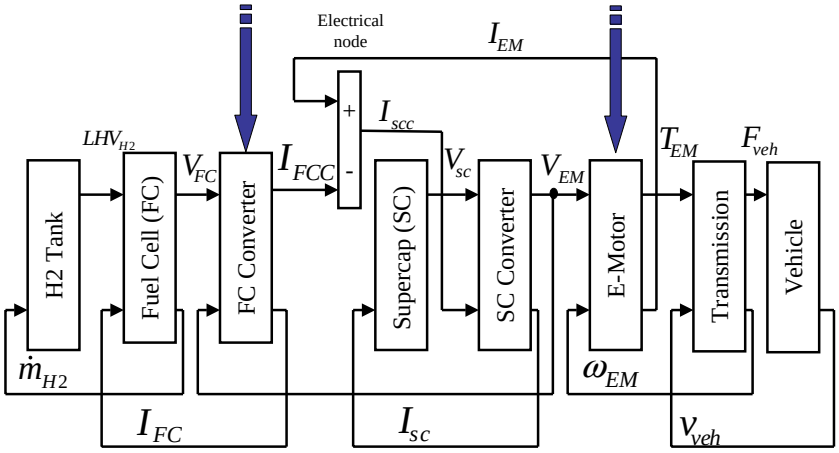

Fig. 3. Powertrain causality flowchart.

Table 2
System constraints

Parameter	Unit	Fuel cell	Supercapacitors
Power	kW	$0<P_{FC}<40$	$-60<P_{SC}<+60$
Current	A	$0<I_{FC}<150$	$-250<I_{SC}<+250$
Voltage	V	$70<V_{FC}<380$	$180<V_{FC}<360$
Power gradient	kW/s	$-5<\Delta P_{FC}<2.5$	—

power flows in all types of vehicles, including conventional, hybrid electric and recently, fuel cell vehicles as well (Rizzoni, Guezennec, Brahma, Wei, & Miller, 2000; Rizzoni, Guzzella, & Baumann, 1999; Boettner, Paganelli, Guezennec, Rizzoni, & Moran, 2002). A model of the vehicle considered was built using a scalable component library. Energy and power flows in the vehicle powertrain were then simulated for numerous driving cycles. Dynamic performance, such as acceleration, top speed, towing capability, gradability, and powertrain efficiency were also evaluated. One important feature of VP-SIM is its respect for the physical causality chain. In other words, the inputs to the model are identical to those of the physical system. This allows to realistically represent the impact of power limitation of the powertrain and of the control on the vehicle performance. Moreover, the control algorithms are directly transferable from the model to the real vehicle and vice versa. All components of the vehicle are available in the library of VP-SIM. Special attention has been devoted to the fuel cell system, which represents the most critical and complex subsystem of the powertrain. The fuel cell VP-SIM model is based on a set of semi-empirical equations, which allow the computation of the fuel cell voltage vs. current characteristics, which have been validated with experimental data. Fig. 4 shows the VP-SIM computed voltage vs. current curves of one cell at an operation pressure of 2 bar_{abs} for the Hy.Power fuel cell configuration.

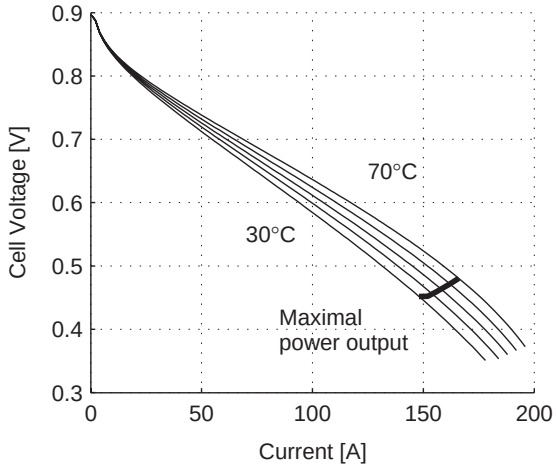

Fig. 4. VP-SIM-computed fuel cell voltage vs. current characteristics for the Hy.Power vehicle.

The VP-SIM model also takes into account the power requirement of the auxiliary components necessary to support the operation of the fuel cell. Realistic efficiency data and control policies have been associated with those components. The model uses conservation-of-energy analyses to compute the heat transfer associated to the fuel cell operation. The heat transfer translates into fuel cell temperature using a simplified thermodynamic fuel cell model. The model has been extensively validated by means of experimental data available from the real powertrain. To conclude this section, Figs. 5 and 6 show the hydrogen consumption and the efficiency vs. net fuel cell power for both the real and the modeled fuel cell system, respectively. Those characteristics, which are given here for steady-state conditions, are representative of the overall performance of the fuel cell system. The average experimental characteristics reasonably match those of the simulations, although in the higher power range a deviation is observed.

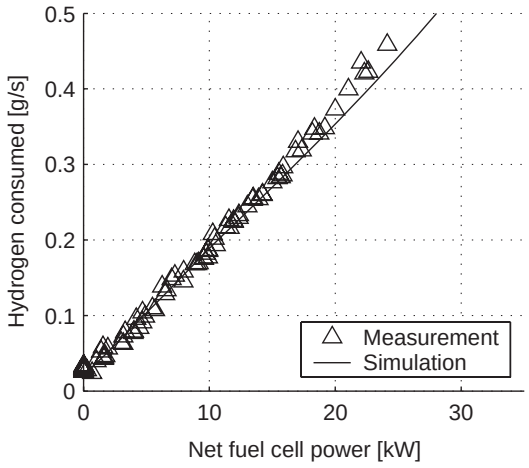

Fig. 5. Hydrogen consumption vs. net fuel cell power.

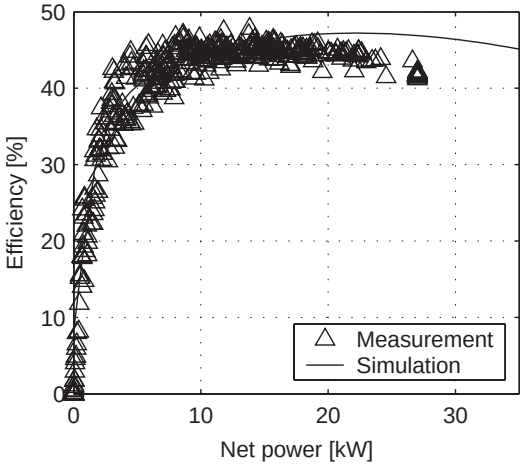

Fig. 6. Fuel cell system efficiency (based on the lower heating value of hydrogen) vs. net fuel cell power.

4. The equivalent consumption minimization strategy (ECMS)

This section is devoted to the control strategy. It is designed to manage the power flows within the vehicle. It is based on a concept of equivalent fuel consumption. For a general and detailed description see Sciarretta, Guzzella, and Onder (2003).

Both the fuel cell and the supercapacitors contribute to the supply of the vehicle power. Hence, the power flow in the DC link $P_{DC}(t)$ is given as follows:

$$P_{DC}(t) = P_{FC}(t) + P_{SC}(t), \tag{1}$$

where $P_{FC}(t)$ is the net power produced by the fuel cell and $P_{SC}(t)$ is the power to or from the supercapacitors. Throughout this paper, the power flow is defined to be "positive" when current is drawn from the fuel cell or supercapacitors (discharge). When current flows into the supercapacitors (charge) it is defined as "negative".

The control variable is the power split factor u that regulates the power distribution among the parallel paths. It is defined as $u(t) = P_{SC}(t)/P_{DC}(t)$. The value $u(t) = 1$ therefore means that all the (positive) power needed at the wheels is provided by the reversible path, or that all the (negative) power available from regenerative braking is taken up entirely by the reversible path. When $u(t) = 0$, it means that all the power is provided by the fuel cell path.

Ideally, the power distribution has to be optimized to minimize the overall hydrogen consumption over a given mission:

$$\text{Min} \sum_{0}^{t_f} P_{H2}(t_k)\Delta t_k, \tag{2}$$

where $P_{H2}(t_k)$ is the hydrogen power needed for the power output of the fuel cell $P_{FC}(t_k)$ at time step Δt_k. It is the product of the hydrogen mass flow rate $\dot{m}_{H2}(t_k)$ and the lower heating value of hydrogen LHV_{H2}. For reasons of clarity, index k is omitted in the following, but t is understood to refer to the time-discrete value t_k.

The main problem with this global minimization criterion is that the whole driving schedule has to be known a priori, thus real-time control cannot readily be implemented.

This drawback may be avoided by using the ECMS, a power distribution control strategy, initially developed for parallel hybrid vehicle applications (Paganelli et al., 2000; Paganelli et al., 2001). It proposes to replace the global criterion by a local one, which appropriately reduces the problem to a minimization of an equivalent fuel consumption at any instance. Thus, for each time t with a time step Δt, the control approach finds the value of the control variable $u(t)$ by minimizing a cost function $J(t)$, defined as

$$J(t) = P_{H2}(t) + s(t)P_e(t). \tag{3}$$

The quantities $P_{H2}(t)$ and $P_e(t)$ are the hydrogen power flow to the fuel cell and the power flow to or from the reversible energy storage (i.e., supercapacitors) in the interval Δt. The factor $s(t)$ facilitates the conversion of the electrical power flow into a chemical power flow, taking into account the efficiency of the power plant. The derivation of $s(t)$ is given below.

The global and the local minimization problems are not identical (Sciarretta et al., 2003). However, the local minimization problem described above can be easily used for real-time control whereas its global counterpart is non-causal and hence non-realizable.

The evaluation of the equivalence factor $s(t)$ represents the core of the ECMS. This parameter influences the system behavior as follows: if $s(t)$ is too large, the use of the energy from the reversible storage tends to be penalized and the fuel consumption increases. If, on the

contrary, $s(t)$ is too small, then the reversible energy use is favored and the supercapacitors are depleted.

The derivation of $s(t)$ is subdivided into three steps. First, two constant equivalence factors, s_{dis} and s_{chg}, are introduced in order to evaluate the fuel equivalent of positive and negative reversible energy use at the end of a drive cycle. Then, by introducing a probability factor $p(t)$, the variable equivalence factor $s(t)$ to be used during the cycle is evaluated as a function of s_{dis} and s_{chg}. Finally, the evaluation of $p(t)$ during real-time operation is presented.

4.1. The concept of equivalent fuel consumption

The procedure described in the following allows the evaluation of the fuel equivalent of the electrical energy use for a given hybrid electric vehicle over a given drive cycle. The procedure requires running the model for various constant values of the control variable. For this purpose the storage capacity of the supercapacitors was artificially increased in order to extend the range of the control variable $u \in [u_{min}, u_{max}]$. At the end of each run, the values of the fuel energy use E^f_{H2} and of the reversible energy use E^f_e over the cycle are collected. These values represent the final (i.e., at the final time of the cycle) values of the cumulative quantities $E_{H2}(t)$ and $E_e(t)$. The values of E^f_{H2} and E^f_e for different runs are plotted in Fig. 7, which refers to the New European drive cycle (NEDC). The pure fuel cell case $u = 0$ is outlined in the plot. The fuel energy used in this case, E^0_{H2}, is the energy that would be used to drive the cycle if no reversible path were present.

For the NEDC cycle, as well as for many other drive cycles (such as ECE, EUDS, FTP75 or JP10-15), it has been observed that the pure fuel cell case separates the curve $E^f_{H2} = f(E^f_e)$ into two segments, which are nearly linear in the range of interest. The slopes of the straight lines that fit the data are labeled s_{dis} and s_{chg}. The linearity arises even if the efficiencies of the parallel paths vary in a nonlinear way depending on the operating point. This may be interpreted as an averaging effect, due to the large number of operating points covered in a driving cycle. s_{chg} refers to the amount of chemical energy (in J) which is spent to store 1 J of electrical energy in the supercapacitors. s_{dis} refers to the amount of chemical energy (in J) which is saved when 1 J of electrical energy is depleted from the supercapacitors. The difference between the numerical values of s_{dis} and s_{chg} results from losses in the reversible (i.e., supercapacitor) path. If the efficiency of the electrical path were unitary, a factor valid for the whole range of operation would result. Thus, an analytical approximation for the curve in Fig. 7 is

$$E^f_{H2} = f(E^f_e) = \begin{cases} E^0_{H2} - s_{dis}E^f_e & \text{if } E^f_e < 0, \\ E^0_{H2} - s_{chg}E^f_e & \text{if } E^f_e > 0. \end{cases} \quad (4)$$

The function $E^f_{H2} = f(E^f_e)$ has been used to define the fuel energy equivalent E^{eq}_e of a variation E^f_e of the electrical energy use from the supercapacitors after a drive cycle. The basic idea is based upon the required self-sustainability of the reversible path: E^{eq}_e has to be zero for a null E^f_e, otherwise it has to represent the fuel energy that will compensate the variation E^f_e in the future. These requirements are fulfilled by the following definition of the fuel energy equivalent (for more details see Sciarretta, Back, & Guzzella, 2002):

$$E^{eq}_e = \begin{cases} s_{dis}E^f_e & \text{if } E^f_e > 0, \\ s_{chg}E^f_e & \text{if } E^f_e < 0. \end{cases} \quad (5)$$

The investigation above does not account for any energy recovered by regenerative braking, E_r. Since the amount of recoverable energy is constant for a given drive, regenerative braking results in a pure horizontal translation of the considered curve, illustrated by the dashed line on Fig. 7. Therefore, the slopes of s_{dis} and s_{chg} are not affected by regenerative braking.

Practical values of the equivalence factors s_{dis} and s_{chg} have been computed for the powertrain considered. They are shown in Table 3 for different drive cycles. Clearly, these values tend to increase for the more demanding driving cycle. As the average power demand increases, the region of fuel cell operation shifts to the low-efficiency, high-power area. Any variation of the power demand thus translates into a corresponding change in fuel cost.

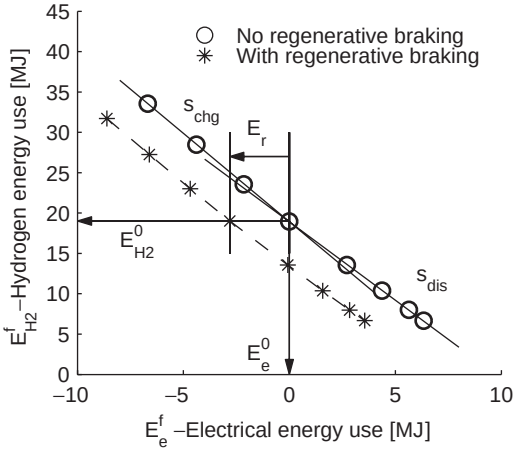

Fig. 7. Fuel energy equivalent of the supercapacitor electrical energy. E^0_{H2} and E^0_e denote the hydrogen energy use and the reversible energy use for the pure fuel cell case $u = 0$.

4.2. The variable equivalence factor

As stated above, the reversible energy use at the end of a drive cycle E^f_e can be converted into an equivalent fuel energy by the equivalence factor s_{dis}, if it is positive, or s_{chg}, if it is negative. During real-time operation, the

Table 3
Equivalence factors for different cycles

Driving cycle	s_{chg}	s_{dis}
NEDC	1.94	2.19
FUDS	2.05	2.30
FHDS	2.00	2.39

NEDC is a combined chassis dynamometer test used for emission testing and certification in Europe. It is composed of four ECE urban driving cycles, simulating city driving, and one extra urban driving cycle (EUDC), simulating highway driving conditions. The federal urban driving schedule (FUDS) and the federal highway driving schedule (FHDS) are used for emission certification testing of cars and light duty trucks in the US.

ECMS uses those values of s_{dis} and s_{chg} that are representative of the current driving conditions. This can be done by storing in the controller certain values that are typical of urban, extra-urban, etc. drive cycles.

Since the quantities s_{dis} and s_{chg} are assumed to be known at every time t during the cycle, they may be used to evaluate the equivalence factor $s(t)$ that converts the quantity $E_e(t)$ into an equivalent fuel energy (Eq. (5)). But the use of s_{dis} and s_{chg} depends on the sign of E_e^f, which cannot be known during real-time operation since the future values of $E_e(t)$ are not known. Therefore, $s(t)$ cannot be replaced with certainty by s_{dis} or by s_{chg}, but is evaluated instead by introducing the estimated probability that $E_e(t)$ will be positive:

$$s(t) = s_{dis}p(t) + s_{chg}[1 - p(t)]. \tag{6}$$

If $p(t) = 1$, it thus follows that $s(t) = s_{dis}$ and if $p(t) = 0$ it follows that $s(t) = s_{chg}$. The problem of the evaluation of $s(t)$ is therefore transferred to the evaluation of $p(t)$.

For the probability evaluation described above, a *time horizon* t^h is defined. It is characterized by a given balance of energy E_{DC}^h required at the DC link level (including both traction and regenerative phases and corresponding to an average typical energy demand over the time horizon), and a corresponding amount of maximum electrical energy available from the fuel cell path E_{FC}^h (corresponding to the potential electrical energy available from the fuel cell if it were to run at full power over the time horizon).

The probability $p(t)$ is calculated as follows (the interested reader is referred to Sciarretta et al. (2002) for more details):

$$p(t) = \frac{E_e(t) + E_{DC}^h}{E_{FC}^h}. \tag{7}$$

For a given powertrain, the maximum power achievable from the fuel cell system, P_{FC}^{max}, is known. Moreover, a typical average power demand P_{DC}^{avg} can easily be assumed. Furthermore, $E_{DC}^h = t^h \cdot P_{DC}^{avg}$ and $E_{FC}^h = t^h \cdot P_{FC}^{max}$. The above equation thus may be rewritten as follows:

$$p(t) = \frac{E_e(t)}{t^h P_{FC}^{max}} + \frac{P_{DC}^{avg}}{P_{FC}^{max}}, \tag{8}$$

where the time horizon t^h becomes the only tuning parameter.

The variable $E_e(t)$ in Eq. (7) provides a feedback of the SOC of the supercapacitors, since it is the time integral of the supercapacitor power and thus describes the deviation in SOC from its initial value. This enforces a natural charge-sustaining operation without the requirement for any additional controller.

The choice of the time horizon t^h depends on the desired aggressiveness of the SOC control and on the capacity of supercapacitors. The shorter the time horizon, the faster a SOC control is achieved. This is intuitively correct since the time required for the compensation of a deviation in SOC increases with the magnitude of the deviation. In other words, the longer the time horizon, the larger are the allowed deviations and the longer is the time required to correct these deviations. Supercapacitors only have a limited capacity compared to batteries. To avoid deviations in the SOC beyond the limitations, a short time horizon has been selected.

4.3. Implementation and practical considerations

In addition to the supercapacitors, the vehicle mass itself is a reversible energy storage system, which stores kinetic energy. In many hybrid vehicles, this storage capability is generally negligible when compared to the capacity of the electrical accumulator. In the vehicle considered, the supercapacitors have been sized to present a usable maximum energy of 1.2 MJ, which is roughly comparable to the kinetic energy stored in the vehicle at the maximum speed of 115 km/h. Thus, in order to achieve maximum benefits from the hybridization, the kinetic energy must be included. On the one hand, at low speed, the supercapacitors should have maximum energy reserve to contribute to the acceleration of the vehicle. On the other hand, at high speed, a low SOC leaves room for kinetic energy recovery during regenerative braking. In other words, reversible energy is permanently available whether it is in electric or in kinetic form. Thus, the reversible energy $E_e(t)$ is extended to include the kinetic energy

$$E_e(t) = E_{SC}(t) + E_r(t).$$

The implementation of the supervisory controller within the vehicle is depicted in the control scheme shown in Fig. 8. In order to consider the recoverable kinetic energy $E_r(t)$ along with energy stored in the supercapacitors $E_{SC}(t)$, the supercapacitors voltage V_{SC} and the vehicle speed v_{veh} are both taken into account when computing the probability $p(t)$.

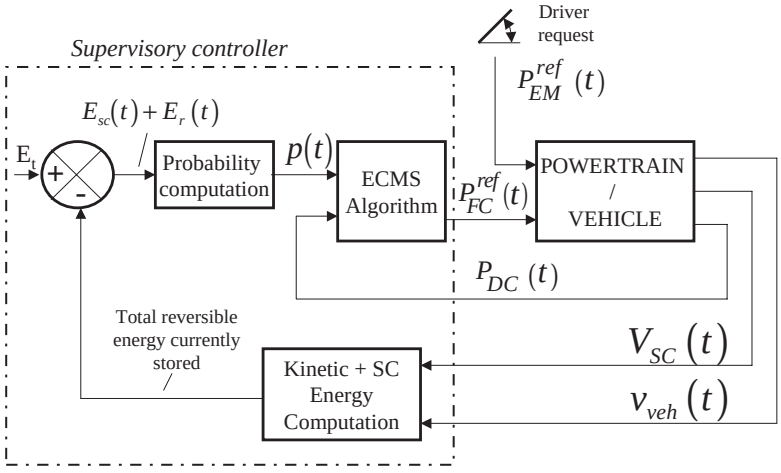

Fig. 8. Implementation of the supervisory ECMS controller in the experimental vehicle.

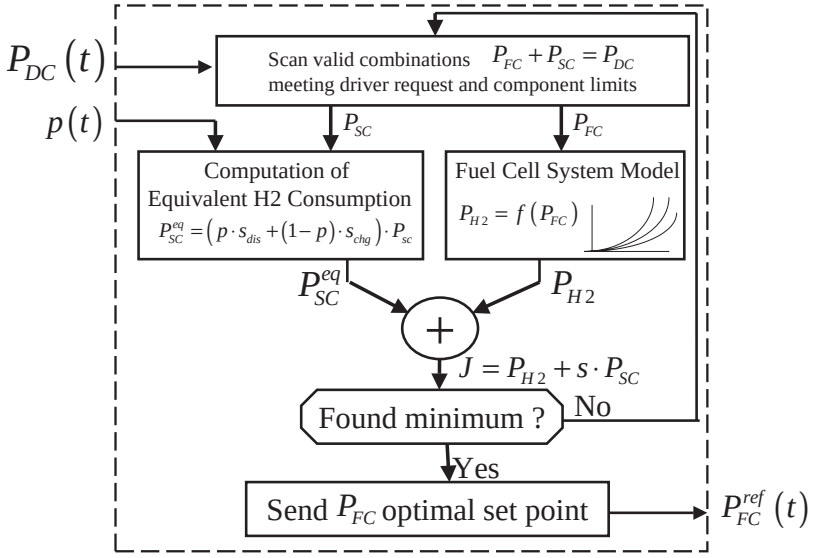

Fig. 9. Principle of the ECMS algorithm applied to the Hy.Power vehicle.

The flowchart of ECMS is sketched in Fig. 9. At each time t with a time step Δt, the following steps are performed:

- The power flow from the DC link to the motor inverter is measured.
- Tentative values of the control variable u are applied in the range $u_{min} \leqslant u \leqslant u_{max}$ (limited by the constraints according to Table 2), with a step of Δu.
- For each tentative value of u, the fuel energy use $P_{H2}(t)\Delta t$ is calculated using data derived from the VP-SIM model, that is parameterized in terms of a fourth-order polynomial. Additionally, using the procedure described in Section 4.2 the reversible energy use $P_e(t)\Delta t$ is calculated.
- The cost function $J(t)$ for the tentative value u is computed as in Eq. (3).
- The control value $u(t)$ is chosen as the tentative value, which yields the minimal value of $J(t)$.

5. Results of experiments

The vehicle was tested on a dynamometer and on the road to verify the predicted operating ability. The highlights of these tests were the trial runs on the Simplon Pass in the Swiss Alps in January 2002.

The NEDC cycle was chosen to obtain comparability of the various energy management strategies. These standard tests were conducted on the dynamometer of the Swiss Federal Laboratories for Materials Testing and Research, EMPA. Table 4 lists vehicle parameters of the dynamometer tests.

Table 4
Parameters for dynamometer testing[a]

Driving cycle	NEDC
Total vehicle mass	1922 kg
Frontal area × drag coefficient	0.6 m^2
Coefficient of rolling resistance	0.1
Constant grade	1%

[a]A 1% slope was applied to take into account the numerous mountain slopes encountered in Switzerland.

Fig. 10 shows measurement data obtained with the ECMS control strategy: The solid line in plot (a) shows the measured vehicle speed, whereas the target speed of the cycle is given by the dashed thin line. The speed profile clearly shows that, the NEDC is a succession of four identical urban sections of about 200 s each, followed by a highway section. As expected, the measurements have shown a repeated system behavior for the four urban sections. For ease of reading, only the

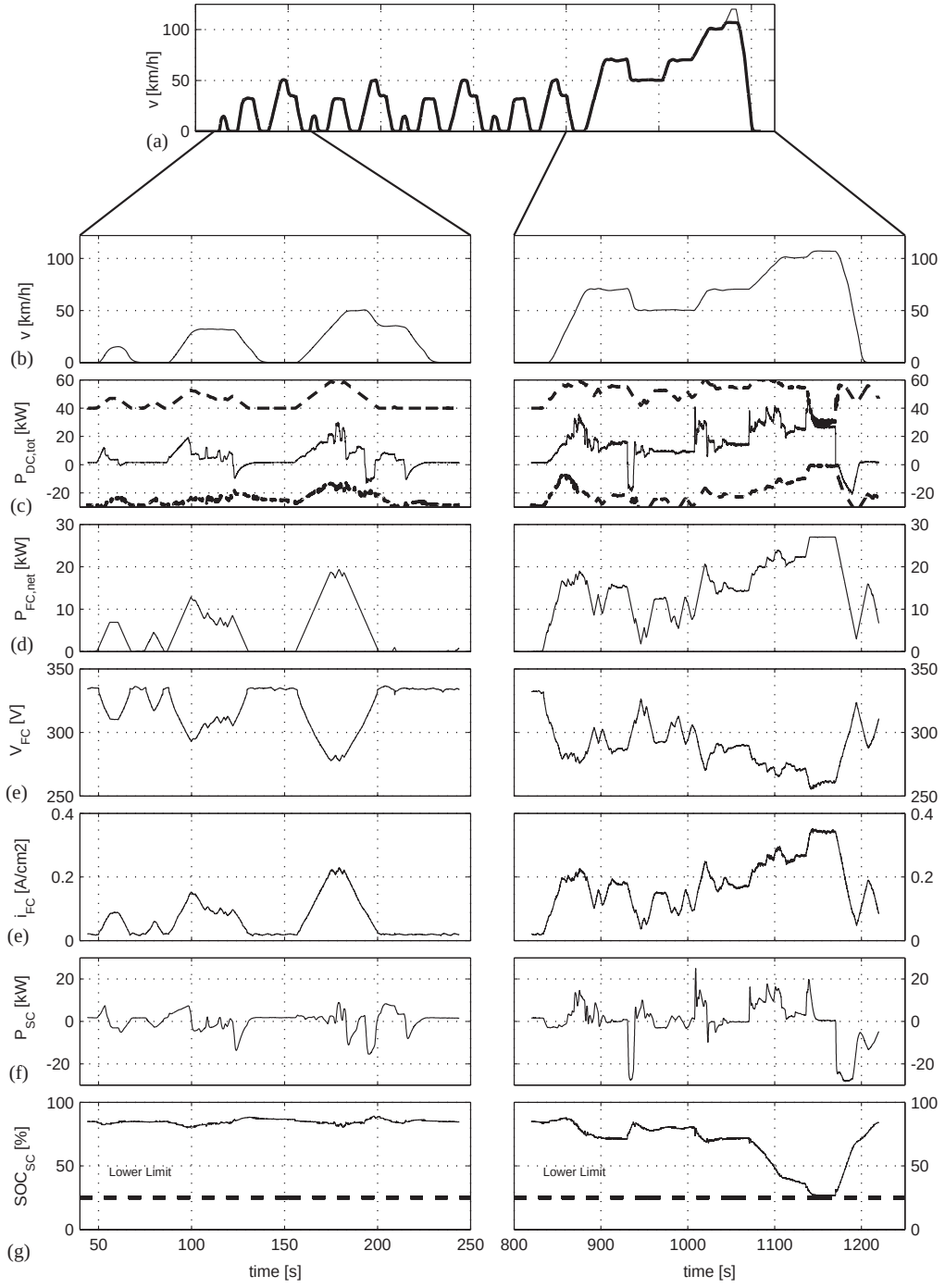

Fig. 10. Dynamometer measurements with ECMS control strategy (a) and (b) vehicle speed, (c) total DC power, (d) net fuel cell power, (e) fuel cell voltage, (f) fuel cell current density, (g) supercapacitor power, (h) supercapacitor SOC.

first urban section (from 40 to 240 s) and the highway section (from 820 to 1220 s) are depicted in plot (b) and in the subsequent plots. Plot (c) shows the total DC power drawn by the vehicle (electric motor and other power consumers within the vehicle). The net power output of the fuel cell system is indicated on plot (d). The net power refers to the power, which is fed into the DC link. The power that is needed to supply the auxiliary components of the fuel cell is not included in this value. The sum of the net power and the power drawn by the auxiliary components is the total fuel cell power, which is the product of voltage and current. The fuel cell voltage and the current density are shown in plots (e) and (f), respectively. The supercapacitors power is shown in plot (g). Negative supercapacitors power values indicate a power flow into the cells, which means that they are being charged. Finally, the supercapacitors SOC is given in plot (h).

As can be seen from plot (a) the vehicle is able to match the speed setpoint well, except for the final acceleration to 120 km/h. The supercapacitors were completely depleted by that time and the vehicle is solely powered from the fuel cells. (Remember that 180 V is the lower operating limit of the supercapacitors corresponding to a 25% SOC.) The 27 kW supplied by the fuel cells are insufficient to accelerate the vehicle to top speed within a reasonable time. The bold dashed lines in plot (c) show the upper and lower power limits that may be requested by the driver.

Similar tests have been performed with the strategy originally implemented in the vehicle. It is a very well tested power management strategy based on a finely tuned 3-D map providing a fuel cell power setpoint as a function of supercapacitors voltage and DC power drawn (Rodatz, Guzzella, & Pellizzari, 2000). Both control strategies offer good transparency for the driver and achieve very similar drivability.

In Table 5, the power consumption of the vehicle is given for the NEDC. Measurements were performed using the ECMS strategy and compared to the original control strategy implemented in the vehicle. Also shown are the results from simulation using the model described above, which match the measurement data reasonably well.

The fuel usage is corrected for (minor) differences in initial and final supercapacitors SOC. The correction is based on the net electricity used converted to equivalent fuel consumption using the equivalence factors introduced in Section 4. Furthermore, the hydrogen usage is converted to equivalent gasoline usage based on the lower heating value of hydrogen and gasoline. This allows to report the results in a more intuitively understandable form.

The fuel efficiency benefit with the ECMS control strategy is not significant. This result may be explained by the system efficiency data in Fig. 6. The efficiency curve is very flat over a large range. A significant gradient exists only at low net power output. Therefore, the room for optimization is very limited in this specific set-up. Simulations have been performed with system configurations that have a less flat efficiency curve. Here substantial improvements can be achieved (see Section 6).

Fig. 11 clearly shows that the ECMS control strategy causes the operating points of the fuel cell to be shifted toward the area of better efficiency. Although a slight improvement is achieved, this does not translate into significant fuel efficiency improvement because of the

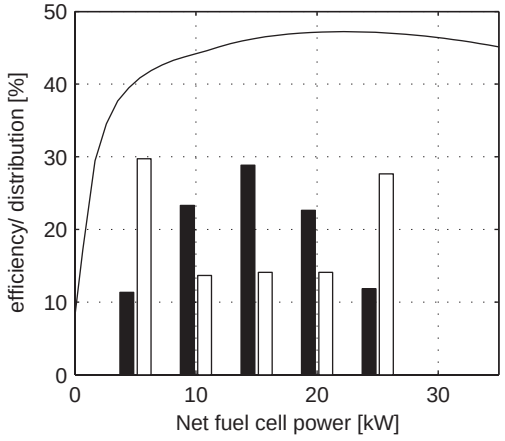

Fig. 11. System efficiency and power distribution of ECMS (black bars) and original control strategy (white bars).

Table 5
Experimental and simulated fuel efficiency for NEDC with 1% slope

	Experimental measurement	Simulation
Original control strategy	6.63 l_{ge}/100 km	6.406 l_{ge}/100 km
	1.816 kg_{H2}/100 km	1.754 kg_{H2}/100 km
ECMS control strategy	6.58 l_{ge}/100 km	6.348 l_{ge}/100 km
	1.801 kg_{H2}/100 km	1.738 kg_{H2}/100 km
Improvement	0.8%	0.9%

l_{ge} = Gasoline equivalent and SOC corrected.

Table 6
Estimated benefit of hybridization on a simulated NEDC driving schedule with Hy.Power configuration

	No slope	With 1% slope
Hydrogen consumption	0.155 kg_{H2}	0.189 kg_{H2}
	5.194 l_{ge}/100 km	6.348 l_{ge}/100 km
	1.422 kg_{H2}/100 km	1.738 kg_{H2}/100 km
Fuel saving due to regenerative braking	−0.025 kg_{H2}	−0.019 kg_{H2}
	−0.907 l_{ge}/100 km	−0.758 l_{ge}/100 km
	−0.248 kg_{H2}/100 km	−0.208 kg_{H2}/100 km

flatness of the efficiency characteristic in the range of interest.

The benefit of regenerative braking on the fuel efficiency has also been estimated using the simulator, Table 6.

6. Perspectives

The simulator has been used to estimate the benefit of ECMS control using an adapted fuel cell system configuration. In this configuration, first the air stoichiometry is limited to 2 (the values in the vehicle are up to 5 at low load) with an air feed at idle of 5 kg/h (as opposed to 24 kg/h in the vehicle). This leads to a significant increase in the net efficiency of the fuel cell, especially at low load, as anticipated in Fig. 12. This new efficiency characteristic has been embedded into the ECMS control strategy in terms of hydrogen consumption versus net output power. Moreover, the power gradient limitation of the fuel cell system has been increased to 5 kW/s as opposed to the currently very conservative 2.5 kW/s and the maximum power limitation has been reset to 40 kW (instead of 27 kW).

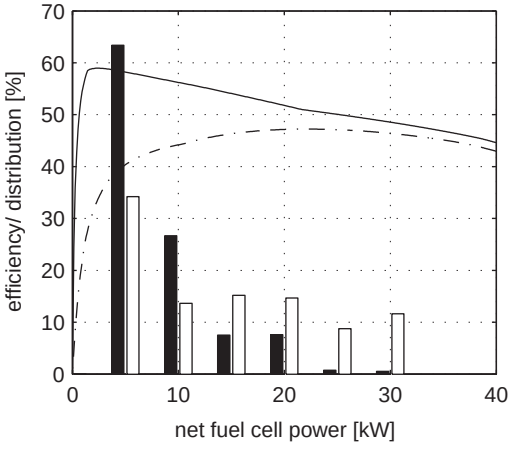

Fig. 12. System efficiency and power distribution of ECMS (black bars) and original control strategy (white bars) for *improved* fuel cell system. The dashed line shows the actual efficiency from Fig. 11.

New simulations with NEDC, FUDS and FHDS driving cycles were conducted with this improved fuel cell system, the remaining of the model being unchanged.

The ECMS control strategy inherently takes into account the efficiency characteristics of the powertrain components. Consequently, it causes the fuel cell operating points to globally shift toward better efficiency conditions. Accordingly, the bar plots in Fig. 12 show that, in the case of ECMS, a larger part of the total energy is produced at the peak efficiency of the system. The overall net power provided by the fuel cell system remains very similar, i.e., 2.303 kWh for the ECMS control strategy and 2.293 kWh for the original control strategy. However, this energy is provided with a slightly better efficiency. Therefore, less hydrogen is used in the case of ECMS. The SOC corrected fuel efficiencies are given in Table 7 for three different driving schedules. A 6.5% improvement is achieved on the urban FUDS driving cycle. As expected, highway-type cycles such as FHDS do not leave much room for optimization since power demand is nearly constant and relatively high.

7. Conclusion

Compared to the original map-based control strategy initially implemented in the vehicle, no significant fuel efficiency improvement is achieved with the ECMS control strategy proposed in this paper. This is because the current fuel cell system does not leave much room for optimization. However, as opposed to the map-based control strategy, ECMS does not require any extended tuning procedure. The only tunable parameter is the time horizon, which defines the dynamic of the SOC. The last section has shown that significant improvement in fuel efficiency may be expected from ECMS, provided that a slightly optimized fuel cell system is implemented. Moreover, the ECMS control strategy embeds a physical model of the fuel cell system in terms of hydrogen consumption vs. net output power characteristics. This feature makes ECMS inherently self-adaptive to achieve full efficiency benefit with any system configuration and operating condition such as

Table 7
Anticipated fuel efficiency improvement with optimized fuel cell system

	NEDC	FUDS	FHDS
Original control strategy fuel efficiency	3.915 l_{ge}/100 km 1.072 kg_{H2}/100 km	3.79 l_{ge}/100 km 1.038 kg_{H2}/100 km	3.40 l_{ge}/100 km 0.93 kg_{H2}/100 km
ECMS fuel efficiency	3.72 l_{ge}/100 km 1.019 kg_{H2}/100 km	3.56 l_{ge}/100 km 0.976 kg_{H2}/100 km	3.34 l_{ge}/100 km 0.916 kg_{H2}/100 km
Improvement	5%	6.5%	2%

l_{ge} = Gasoline equivalent and SOC corrected.

temperature. ECMS also offers a very natural way to sustain the supercapacitors SOC within reasonable limits.

Acknowledgements

Financial support by the Swiss Federal Energy Office and by AMAG Schweiz AG is gratefully acknowledged.

Appendix

In this paper, the fuel cell system efficiency is based on the lower heating value of hydrogen and the net electrical power output (fuel cell electrical power minus parasitic loads of auxiliary units in the fuel cell system: air compressor, cooling, etc.) and is defined as

$$\eta_{FC} = \frac{P_{FC} - P_{Aux}}{\dot{m}_{H2} LHV_{H2}},$$

where $\dot{m}_{H2}$ is the hydrogen consumed by the electrochemical reaction, LHV_{H2} the lower heating value, P_{FC} the electric power output of the fuel cells and P_{Aux} the power drawn by the fuel cell system auxiliaries.

The hydrogen consumption is referred to as the amount of hydrogen actually consumed in the fuel cell reaction. Purged hydrogen is not accounted for. It is calculated as follows:

$$\dot{m}_{H2} = \frac{i_{FC} M_{H2} N_{cells} A_{FC}}{2F},$$

where i_{FC} is the fuel cell current density, M_{H2} is the molecular weight of hydrogen, N_{cells} is the number of individual cells, A_{FC} is the active area of each cell and F is the Faraday's constant.

The supercapacitor efficiency if defined as follows:

$$\eta_{SC} = \begin{cases} (P_{SC} + R_{SC} I_{SC}^2)/P_{SC} & \text{if } P_{sc} < 0, \\ P_{SC}/(P_{SC} + R_{SC} I_{SC}^2) & \text{if } P_{sc} > 0. \end{cases}$$

For reasons of clarity, various efficiencies have been neglected in this paper. However, they are included in the control strategy.

References

Boettner, D., Paganelli, G., Guezennec, Y., Rizzoni, G., & Moran, M. J. (2002). Proton exchange membrane fuel cell system model for automotive vehicle simulation and control. *ASME Journal of Energy Resources Technology*, *124*, 20–27.

Brahma, A., Guezennec, Y., & Rizzoni, G. (2000). Optimal energy management in series hybrid electric vehicle. *Proceedings of American control conference* 2000, Chicago, USA.

Delprat, S., Guerra, T. M., Paganelli, G., Lauber, J., & Delhom, M. (2001a). Control strategy optimization for an hybrid parallel powertrain. *Proceedings of American control conference 2001*, Arlington, USA (pp. 1315–1320).

Delprat, S., Guerra, T. M., & Rimaux, J. (2001b). Optimal control of a parallel powertrain: From global optimization to real-time control strategy. *Proceedings of the electric vehicle symposium*, EVS18, Berlin, Germany.

Dietrich, P., Büchi, F.N., Ruge, M., Tsukada, A., Scherer, G.G., Kötz, R., Müller, S., Bärtschi, M., Rodatz, P., & Garcia, O. (2001). Fuel cells for transportation—a pilot fuel cell propulsion system. *Proceedings of EAEC European automotive congress*, Bratislava, Slovakia.

Johnson, V., Wipke, K., & Rausen, D. (2000). *HEV control strategy for real-time optimisation of fuel economy and emissions*. SAE Technical Paper 2000-01-1543.

Kötz, R., Bärtschi, M., Büchi, F.N., Gallay, R., & Dietrich, P. (2002). HY.POWER—a fuel cell car boosted with supercapacitors. *Proceedings of the 12th international seminar on double layer capacitors and similar energy storage devices*, Deerfield Beach, USA.

Lin, C., Filipi, Z., Wang, Y., Louca, L., Peng, H., Assanis, D., & Stein, J. (2001). *Integrated, feed-forward hybrid electric vehicle simulation in SIMULINK and its use for power management studies*. SAE Technical Paper 2001-01-1334.

Ogburn, M., Nelson, D. J., Luttrell, W., King, B., Postle, S., & Fahrenkrog, R. (2000). *Systems integration and performance issues in a fuel cell hybrid electric vehicle*. SAE Technical Paper 2000-01-0376.

Paganelli, G., Ercole, G., Brahma, A., Guezennec, Y., & Rizzoni, G. (2001). General supervisory control policy for the energy optimization of charge-sustaining hybrid electric vehicles. *Special Issue of JSAE Review—Society of Automotive Engineers of Japan (JSAE)*, *22*(4), 511–518.

Paganelli, G., Guerra, T. M., Delprat, S., Santin, J. J., Combes, E., & Delhom, M. (2000). Simulation and assessment of power control strategies for a parallel hybrid car. *Journal of Automobile Engineering*, *214*, 705–718.

Rizzoni, G., Guezennec, Y., Brahma A., Wei, X., & Miller, T. (2000). VP-SIM: A unified approach to energy and power flow modeling simulation and analysis of hybrid vehicles. *Proceedings of the SAE future car congress paper no. 2000-01-1565*, Crystal City, USA.

Rizzoni, G., Guzzella, L., & Baumann, B. (1999). Modeling and design optimization of hybrid vehicles. *IEEE/ASME Transactions on Mechatronics*, *4*(3), 246–257.

Rodatz, P., Garcia, O., Guzzella, L., Büchi, F.N., Bärtschi, M., Tsukada, A., Dietrich, P., Kötz, R., Scherer, G.G., & Wokaun, A. (2003). *Performance and operational characteristics of a hybrid vehicle powered by fuel cells and supercapacitors*. SAE Technical Paper 2003-01-0418.

Rodatz, P., Guzzella, L., & Pellizzari, L. (2000). System design and supervisory controller development for a fuel-cell vehicle. *Proceedings of the first IFAC conference on mechatronic systems.* Darmstadt, Germany.

Sciarretta, A., Back, M., & Guzzella, L. (2002). Optimal control of parallel hybrid electric vehicles. *IEEE Transactions on Control Systems Technology*, accepted for publication.

Sciarretta, A., Guzzella, L., & Onder, C. (2003). On the power split control of parallel hybrid vehicles: From global optimization towards real-time control. *at—Automatisierungstechnik*, *51*(5), 195–203.

Seiler, J., & Schröder, D. (1998). Hybrid vehicle operating strategies. *Proceedings of the electric vehicle symposium. EVS15*, Brussels, Belgium.

Wipke, K., Markel, T., & Nelson, D.J (2001). Optimizing energy management strategy and degree of hybridization for a hydrogen fuel cell SUV. *Proceedings of the electric vehicle symposium. EVS18*, Berlin, Germany.